

Observing Annual Trends in Vehicular CO₂ Emissions

Jinsol Kim, Alexander J. Turner, Helen L. Fitzmaurice, Erin R. Delaria, Catherine Newman, Paul J. Wooldridge, and Ronald C. Cohen*



Cite This: *Environ. Sci. Technol.* 2022, 56, 3925–3931



Read Online

ACCESS |



Metrics & More

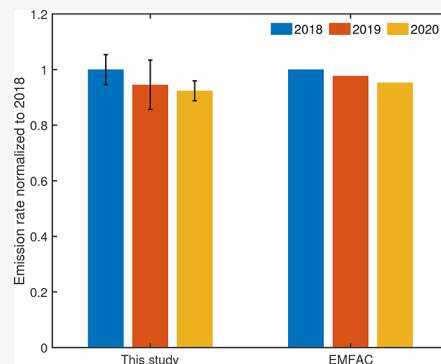


Article Recommendations



Supporting Information

ABSTRACT: Transportation emissions are the largest individual sector of greenhouse gas (GHG) emissions. As such, reducing transportation-related emissions is a primary element of every policy plan to reduce GHG emissions. The Berkeley Environmental Air-quality and CO₂ Observation Network (BEACO₂N) was designed and deployed with the goal of tracking changes in urban CO₂ emissions with high spatial (~1 km) and temporal (~1 hr) resolutions while allowing the identification of trends in individual emission sectors. Here, we describe an approach to inferring vehicular CO₂ emissions with sufficient precision to constrain annual trends. Measurements from 26 individual BEACO₂N sites are combined and synthesized within the framework of a Gaussian plume model. After removing signals from biogenic emissions, we are able to report normalized annual emissions for 2018–2020. A reduction of $7.6 \pm 3.5\%$ in vehicular CO₂ emissions is inferred for the San Francisco Bay Area over this 2 year period. This result overlaps with, but is slightly larger than, estimates from the 2017 version of the California Air Resources Board EMFAC emissions model, which predicts a 4.7% decrease over these 2 years. This demonstrates the feasibility of independently and rapidly verifying policy-driven reductions in GHG emissions from transportation with atmospheric observations in cities.



KEYWORDS: greenhouse gas, fossil fuel, fluxes, fuel efficiency, dense sensor network

1. INTRODUCTION

In 2006, California passed Assembly Bill 32 (AB 32), the Global Warming Solutions Act, which requires the state to reduce its greenhouse gas (GHG) emissions by 40% of 1990 emissions by the year 2030. Transportation emissions are the largest individual sector of GHG emissions, and California aims to limit GHG emissions in this sector to 103–111 MMTCO₂e by 2030.¹ In 2017, transportation emissions were 170 MMTCO₂e.² If the reduction occurs linearly, meeting this goal would require a 3% yr⁻¹ decrease. On a regional scale, the Bay Area Air Quality Management District is a nine-county intergovernmental agency with the local authority to support and track progress toward the state's goals. Its stated plans to reduce transportation GHG emissions include a transition to lower GHG emissions while maintaining an economically mobile workforce with action items that include supporting the transition from current vehicle technologies to zero and low GHG emission vehicles, expanding use of mass transit systems, and reducing vehicle miles traveled.³

Our understanding of urban CO₂ emissions currently relies most heavily on a combination of methods based on socioeconomic data and process-level data for individual activities. For example, measurements of the fuel efficiency of a wide suite of individual vehicle types are combined with socioeconomic data about the location of driving, total distance traveled, and the types of vehicles on different roads to estimate total vehicular CO₂ emissions. Another example is

relocating regional fuel consumption data using socioeconomic data, converting fuel sales volume to an equivalent mass rate of CO₂ emissions. The mixture of methods and data sources makes it difficult to quantify the uncertainties in such estimates. One study rigorously evaluating local scale emission models showed that the uncertainty of total emissions and the contribution of individual source sectors to that total is too large to evaluate the effectiveness of the policy related to urban CO₂ emission reduction.⁴

Inferring emissions from the observations of atmospheric CO₂ and other GHGs are a direct method for understanding urban GHG emissions with different uncertainties from approaches based on economic data. To date, most projects using ambient observations have focused on demonstrating the capability of using observations to estimate emissions for a moment in time (or a year). For example, aircraft mass balance measurements were used to estimate total emissions from Indianapolis in 2014 by making observations upwind and downwind of the city and providing an estimate of emissions

Received: October 18, 2021

Revised: March 10, 2022

Accepted: March 11, 2022

Published: March 24, 2022



from the city on the days of those flights.^{5,6} A few studies have looked at interannual trends. Newman et al. (2016),⁷ for example, looked at trends from 2006–2013 and reported a 10% decrease in fossil fuel CO₂ during the 2008 recession. More sophisticated syntheses of prior emission estimates, observations, and meteorological models have been used in ways that optimize the emission model and provide longer-term emission estimates.^{8–11} Most of the studies mentioned above typically consist of 2–15 observing sites with state-of-the-art instruments that are calibrated frequently with gravimetric gas standards. These approaches are labor-intensive.

The Berkeley Environmental Air-quality and CO₂ Observation Network (BEACO₂N)^{12–15} is designed to observe and map short- and long-term variation in both GHG and air quality emissions. The BEACO₂N observing system is designed to produce maps of urban air with ~2 km pointwise spatial resolution while minimizing both capital and operating costs. Nodes in the network include measurements of CO₂, CO, NO₂, NO, O₃, and aerosol. The measurement system aims to provide detailed maps of concentration variations within a city, offering a direct response to concerns about environmental justice and equity in emission reductions, especially those that affect both CO₂ and related air quality emissions such as CO, NO_x, and aerosol. The current network includes about 45 nodes in the San Francisco Bay Area, 12 nodes in Los Angeles, and 12 (soon to be 20) nodes in Glasgow, Scotland. Among our goals in establishing and maintaining these networks is to enable an understanding of trends and the reporting to policy makers about the extent to which the policy tools they are implementing are having the intended effects on both GHG and air quality emissions.

The advantages of a dense network such as the BEACO₂N were evaluated by comparing the relative abilities of instruments of roughly equal capital investment—three state-of-the-art instruments versus 25 BEACO₂N-like nodes (the number of BEACO₂N nodes that were installed in 2016)—as constraints on an inverse model.¹⁶ The BEACO₂N-like system outperformed the alternative for characterizing a point, line, or area source within an urban region. In a first effort to describe changes in emissions over time with the BEACO₂N, the network observations have been combined with a formal inverse model to deliver an estimate of total CO₂ reductions in a region of the San Francisco Bay Area during the COVID-19 shelter-in-place.¹⁷ The observation/modeling system was able to allocate those reductions on a map with ~1 km of fidelity.

In addition to this sophisticated and computationally intensive inverse modeling approach, it is advantageous to explore simpler methods of analysis. The ability of the BEACO₂N to constrain policy-relevant trends in highway traffic emissions has been previously demonstrated using a multiple linear regression method to decompose CO₂ signals into emissions from vehicles and the influence of meteorology.¹⁵ That paper underscored that each individual site in the BEACO₂N carries information about emissions on the highways. Here, we present an advance on this approach. Sites in the network are combined within the framework of a Gaussian plume model to yield higher signal-to-noise and constraints on annual trends in urban CO₂ emissions from the vehicle sector.

2. MATERIALS AND METHODS

2.1. Measurements. We use a high-density observing system, the BEACO₂N, that was designed and deployed with the goal of tracking changes in urban CO₂ emissions with ~1 km spatial resolution and a time resolution of ~1 hr. A detailed description of the design and deployment of the BEACO₂N can be found elsewhere^{13–15} and in the [Supporting Information](#), Section 1. The raw 5 s CO₂ concentration at each node was processed into calibrated, bias-corrected, dry-air mole fractions using in-node temperature, pressure, and relative humidity observations and in-network reference measurements and averaged to hourly means as described in Shusterman et al. (2016),¹⁴ including the extensive characterization of temperature-dependent instrument responses described in Delaria et al. (2021).¹² The precision of the hourly observations is estimated to be ±0.5 ppm and the accuracy of 1–2 ppm.^{12,14,15} We utilize CO₂ observations from 26 San Francisco Bay Area sites that were active for at least 3 months between January 2018 and December 2020 (see [Figures 1 and 2](#)).

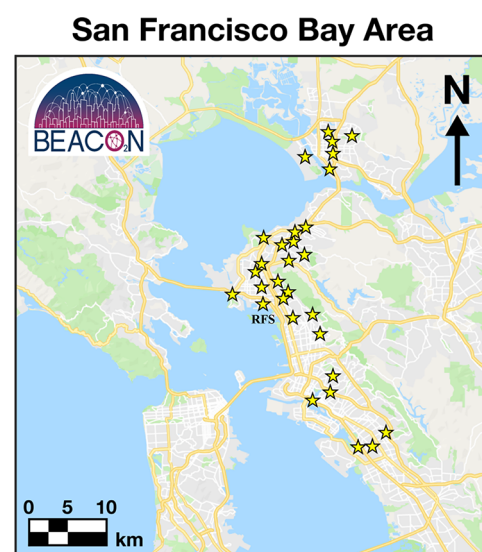


Figure 1. Map of the San Francisco Bay Area showing the BEACO₂N node locations used in this study.

Traffic information is available through the Caltrans Performance Measurement System (PeMS; <http://pems.dot.ca.gov>), operated by the California Department of Transportation. Hourly vehicle flow and vehicle speed data from the monitors at highway locations upwind and closest to the relevant BEACO₂N sites are collected and summed across all the lanes and directions. Data reported by Caltrans is often filled with model output when observations are not reported by the sensors. Only the hours with more than 50% directly measured were used to exclude those moments that are almost entirely traffic model. Because the emission rate of an individual vehicle varies with speed, we focus here on the most common mode of traffic and include only those times when the average vehicle speed was faster than 30 mph. Reduced traffic demand in 2020 due to the COVID shutdown led to more total time at speeds >30 mph, particularly during rush hours.

2.2. Gaussian Plume Method. The concentration enhancement for CO₂, $C_{\text{enh}}(x, z)$ [kg CO₂ m⁻³], at a distance

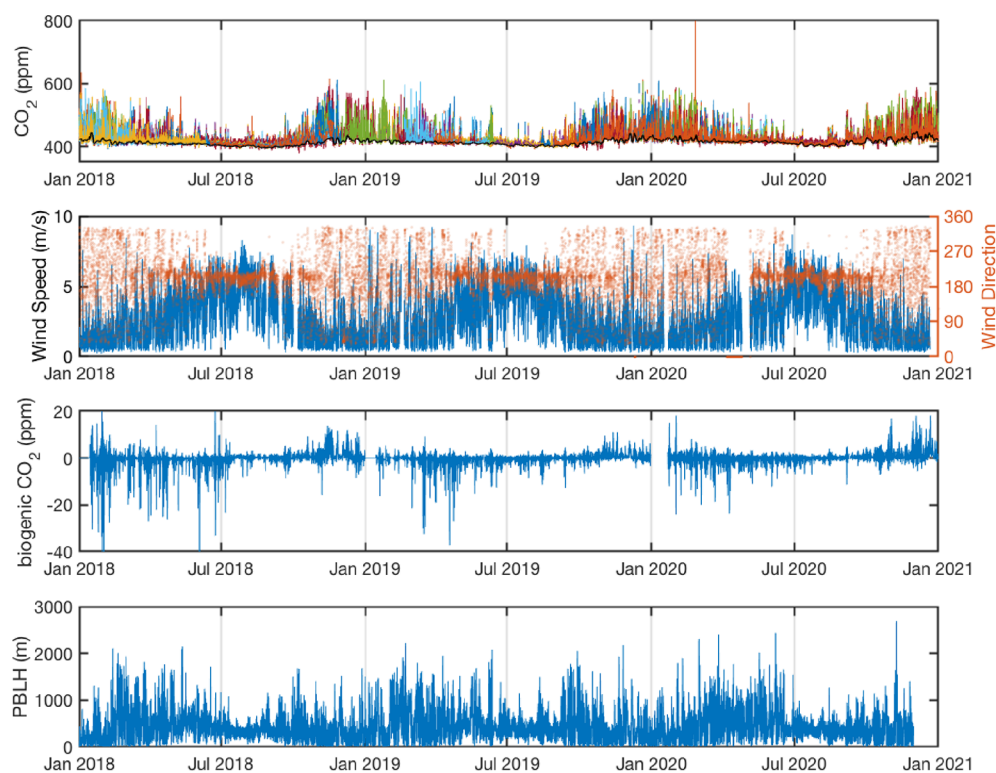


Figure 2. Observation of (a) CO₂ from all the BEACO₂N sites used in this study and the (b) wind at the RFS supersite. Different colors indicate different BEACO₂N sites, and the black line represents the background CO₂ in the top panel. Network average of (c) biogenic CO₂ enhancement from the HRRR-STILT model combined with biogenic fluxes, and the (d) PBLH from the ECMWF ERAS model.

x and height z , within a Gaussian plume flowing from an infinite line source oriented along the y axis (e.g., a highway), is expressed as eq 1, which is an integration of the Gaussian plume model for a point source along a line source

$$C_{\text{enh}}(x, z) = \frac{Q}{\sqrt{2\pi} \sigma_z(x) \times U} \left[\exp\left(-\frac{(z+H)^2}{2\sigma_z^2(x)}\right) + \exp\left(-\frac{(z-H)^2}{2\sigma_z^2(x)}\right) \right] \quad (1)$$

The derivation assumes reflection at the surface. The line source is taken to be at a height H [m]. Q [kg CO₂ m⁻¹ s⁻¹] is the emission rate along the highway, U [m s⁻¹] is the wind speed perpendicular to the highway, and the dispersion parameter $\sigma_z(x)$ [m] is the standard deviation of the concentration distributed in the z direction at the location x .

We simplify this expression by approximating highways in the San Francisco Bay Area as infinite line sources on the ground ($H = 0$), as most of the highways referred to in this study are not elevated

$$C_{\text{enh}}(x, z) = \frac{2Q}{\sqrt{2\pi} \sigma_z(x) \times U} \left[\exp\left(-\frac{z^2}{2\sigma_z^2(x)}\right) \right] \quad (2)$$

BEACO₂N sites are treated as if they are on the ground ($z = 0$), as BEACO₂N nodes used in this study are located less than 10 m above the ground. These small differences from $z = 0$ are inconsequential for most of the BEACO₂N sites used in this study (see Supporting Information Section 2). The emission rate Q [kg CO₂ m⁻¹ s⁻¹] of the highway line source can be expressed as a product of the emission rate of the average

vehicle q [kg CO₂ m⁻¹ per vehicle] and the observed flow rate of vehicles (VPS, in vehicles per second)

$$Q = q \times \text{VPS} \quad (3)$$

Based on the assumptions mentioned above, we can rearrange eq 2 to show the ratio of $C_{\text{enh}}(x)$ divided by VPS as a function of emissions (q)

$$\frac{C_{\text{enh}}(x)}{\text{VPS}} = \frac{2q}{\sqrt{2\pi} \times \sigma_z(x) \times U} \quad (4)$$

Gaussian plume models applied to urban emissions commonly use an empirically parameterized dispersion parameter $\sigma_z(x)$. Choi et al. (2014)¹⁸ evaluated several semiempirical choices for connecting meteorological parameters to plume properties. In their analysis, Q and dispersion coefficients were free variables determined by fitting a Gaussian expression to observed concentrations at locations downwind of a line source. They found the dispersion coefficients to be dependent on temperature, wind speed, and wind direction under stable nocturnal conditions. We adopt a similar approach to explain the daily variation of dispersion. We parameterize $\sigma_z(x)$ with Briggs' expression¹⁹ as in eq 5 (see Supporting Information Section 4 for more details) and set α and β as free variables.

$$\sigma_z(x) = \frac{\alpha x}{1 + \beta x} \quad (5)$$

Combining eqs 4 and 5 yields

$$\frac{C_{\text{enh}}(x)}{\text{VPS}} = \frac{2}{\sqrt{2\pi}} \frac{1}{U} \frac{q}{\alpha} \frac{1 + \beta x}{x} \quad (6)$$

The dimensionless dispersion coefficients α and β determine the shape of the decaying plume. α has a dominant effect close to the highway and the importance of β increases at long distance. We use the wind speed as measured at the RFS supersite (see Figure 2).

This leaves us with two unknowns: q/α and β in eq 6. To solve for the unknowns, we begin by recalling the strong correlation of $C_{\text{enh}}(x)$ and VPS throughout the BEACO₂N domain as described by Shusterman et al. (2018).¹⁵ The slope of the linear regression between $C_{\text{enh}}(x)$ and VPS was observed to vary and to be steeper near the highway than at sites remote from the highway. Here, we fit $C_{\text{enh}}(x)$ versus VPS at all the distances, x , from the highway to derive the slope $\frac{C_{\text{enh}}}{\text{VPS}}(x)$ (see Figure 3). Then, we fit $\frac{C_{\text{enh}}}{\text{VPS}}(x)$ vs x to eq 6, deriving q/α and β from the fit.

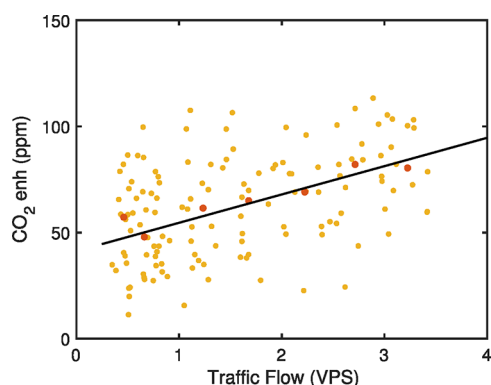


Figure 3. Example of derivation of the slope $\frac{C_{\text{enh}}}{\text{VPS}}(x)$. The red points indicate the median CO₂ enhancement observed in each 0.5 vehicles s⁻¹ traffic flow increment; the black solid line indicates the linear regression through the binned medians.

In this analysis, the local enhancement, $C_{\text{enh}}(x)$, is defined as the total enhancement of CO₂ at each location above a single network-wide background. The background is defined as the 3 day running mean of the lowest fifth percentile of BEACO₂N observations at all the nodes in the network. In the BEACO₂N domain, the 3 day running mean represents the background concentration without a diurnal cycle and includes some synoptic variation and seasonal variation. As the wind is

dominantly blowing from the ocean (see Figure 2) and there is little land between the network and the coast, this background is little influenced by the local biosphere.

A critical element of this analysis is reducing the uncertainty in the annual emissions estimate by reducing the uncertainty in the response of local CO₂ enhancement to traffic emissions and dispersion coefficients. The local CO₂ enhancement is also affected by emissions from other anthropogenic sources and both emissions from and uptake into the urban biosphere. Anthropogenic sources are dominant in the region, with traffic and point sources, including industrial and energy sectors, contributing 41% and 40%, respectively.³ Point sources are thought to operate 24/7 with no diurnal variation in their emissions. Deriving the slope $\frac{C_{\text{enh}}}{\text{VPS}}(x)$ removes most of the influence of these other sources, which exhibit different daily temporal variations from traffic emissions. However, biogenic emissions are anticorrelated with traffic emissions. The biogenic fluxes are positive at night due to respiration and negative during the day, representing photosynthesis. In order to partially mitigate the portion of the local biospheric influence that is anticorrelated with traffic, CO₂ emissions and uptake from the biosphere are predicted and subtracted from the total CO₂ enhancement (see Figure 2 and Supporting Information Section 3).

The dispersion parameter $\sigma_z(x)$ and thus the associated parameters α and β are known to depend on atmospheric stability classes with different wind speeds, radiation, cloud cover, and planetary boundary layer height (PBLH). We focus on the main driver of observed variation, the PBLH. Estimates of the PBLH (see Figure 2) are taken from the 0.25° by 0.25° resolution ECMWF ERA5 model.²⁰ We perform a separate analysis at 20 quantiles of the reanalysis PBLH using the averaged wind speed for each of these intervals as the value for U to fit eq 6. The effect of the PBLH variation on the dispersion parameter $\sigma_z(x)$ and thus the associated parameters α and β is further discussed in the Supporting Information, Section 4.

The relationship between the response of local CO₂ enhancement to traffic emissions and the PBLH is shown in Figure 4. The figure shows a normalized sensitivity where all the values are a ratio of the CO₂ enhancement/vehicle/s at a specific PBLH and location to the value for that same quantity at a PBLH between 100 and 215 m at that same site. The slope

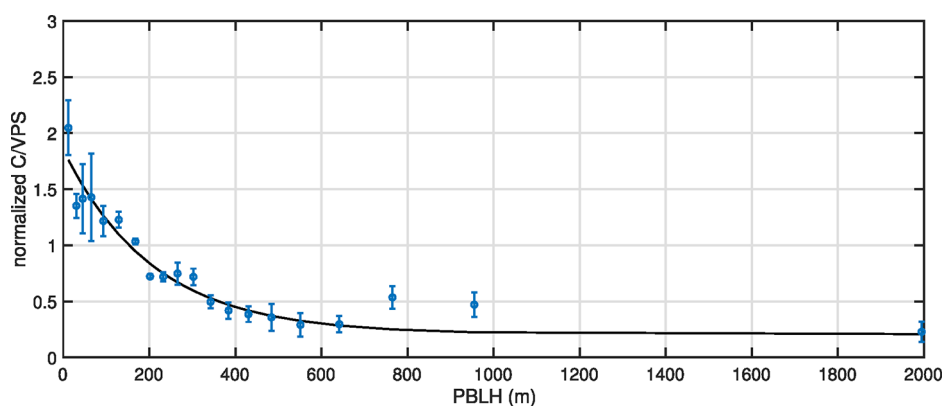


Figure 4. Sensitivity of the local CO₂ enhancement (C) to the number of vehicles (VPS) versus PBLH. The data are normalized by the value at the PBLH between 100 and 215 m of each site. The median of all the sites in the network is indicated with the circle, and the whiskers represent the 1 σ variance. A fit using an exponential function (Equation 7) is shown (black line).

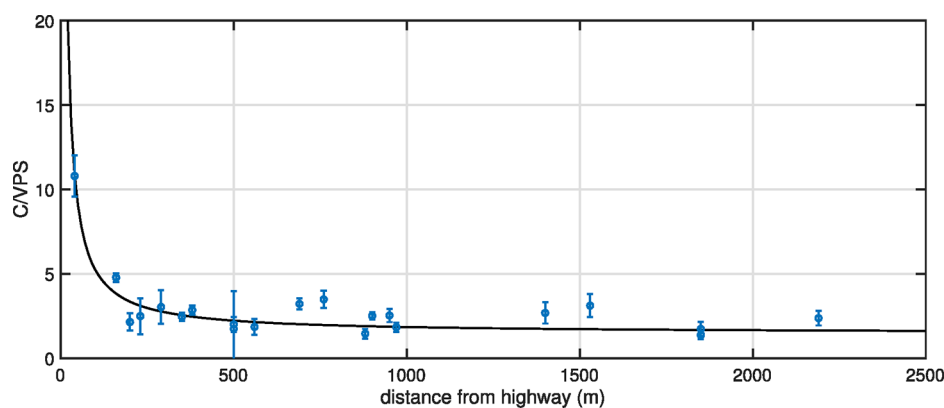


Figure 5. Sensitivity of the local enhancement of CO₂ (C) to vehicle flow (VPS) versus distance from the highway (m) at the PBLH 100–215 m from 2018 through 2020. The median over the range of the PBLH at each site is the circle, and the whiskers represent the 1σ variance. A fit to the decay of C/VPS versus distance using a Gaussian plume model (eq 5) with $q/\alpha = 2006$ (in 10^{-6} kg CO₂ m⁻¹ per vehicle) and $\beta = 0.0052$ is shown in the black line.

of the CO₂ enhancement with vehicle flow decreases at higher PBLH. The higher PBLH is also correlated with higher wind speeds and larger dispersion coefficients. The observed relationship between local CO₂ enhancement, vehicle flow, and the PBLH can be described with an exponential function, eq 7

$$\frac{C_{\text{enh}}(x, \text{PBLH})}{\text{VPS}} / \frac{C_{\text{enh}}(x, 100 - 215 \text{ m})}{\text{VPS}} = (1.644e^{-0.004772 \times \text{PBLH}} + 0.2075) \quad (7)$$

We find a remarkably strong correspondence between the observed and predicted $C_{\text{enh}}/\text{VPS}$. Equation 7 explains 92% of the variability, and the prediction fits most observations to within the uncertainty. Although it is possible that some meteorological effect other than the PBLH is driving the variability we observe, our analysis suggests those terms are correlated with the PBLH, and thus it is sensible to use the PBLH as the effective controlling parameter in the analysis.

Taking the ratio of the slope $\frac{C_{\text{enh}}}{\text{VPS}}(x, \text{PBLH})$ and eq 7 yields the sensitivity of the local CO₂ enhancement to vehicle emissions at any PBLH to the reference PBLH of 100–215 m. These values over the full range of the PBLH are then combined at each site, and the different sites are arranged as a function of distance from the nearest highway line source (see Figure 5). Then, we fit $\frac{C_{\text{enh}}}{\text{VPS}}(x, 100 - 215 \text{ m})$ vs x to eq 6 and find q/α and β .

3. RESULTS AND DISCUSSION

The relationship between CO₂ concentration and highway traffic flow is coherent throughout the network, and the influence follows a quantitative relationship consistent with Gaussian dispersion: near highway sites respond strongly to the highway and distant ones, less so (see Figure 5). We first fit the observations with q/α and β as free variables. Analyzing the data from 2018 through 2020 simultaneously yields a value for q/α of 2006×10^{-6} kg CO₂ m⁻¹ per vehicle and β of 0.0052 ± 0.0020 , respectively. α is expected to lie in the range ~ 0.05 and ~ 0.2 based on the relationship between α and β found by Choi et al. (2014)¹⁸ and our determination of $\beta = 0.0052$ in the BEACO₂N domain. The relationship between α and β found by Choi et al. applies to geometries where the sampling transect is higher than or lower than the highway. The

BEACO₂N nodes are both above ($\alpha = 0.05$) and below ($\alpha = 0.2$) the relevant highways. Assuming a value for α that spans that range, q is estimated to be $100\text{--}400 \times 10^{-6}$ kg CO₂ m⁻¹ per vehicle. The mobile emission rate predicted using the 2017 version of the California Air Resources Board (CARB) EMFAC model²¹ is 227×10^{-6} kg CO₂ m⁻¹ per vehicle for on-road traffic from 2018 through 2020. Although our estimate is consistent, the uncertainty due to our inability to narrow the range of α is large. However, α and β are expected to be constant over time. Analyzing the 3 years of observations separately, we find β of 0.0041 ± 0.0017 , 0.0079 ± 0.0050 , and 0.0052 ± 0.0016 for 2018, 2019, and 2020, respectively. Because the difference between the 3 years is insignificant, we fix β to be 0.0052 as derived from the combined analysis of all the 3 years. This constant β induces constant α according to the relationship between α and β described by Choi et al. (2014).¹⁸ Assuming a constant value for α , we derive normalized emissions relative to 2018 by taking the ratio of q/α for each year and comparing to the q/α of 2018.

Figure 6 shows these BEACO₂N-derived normalized emission rates for 2018, 2019, and 2020 and compares them to normalized predictions from the CARB EMFAC 2017

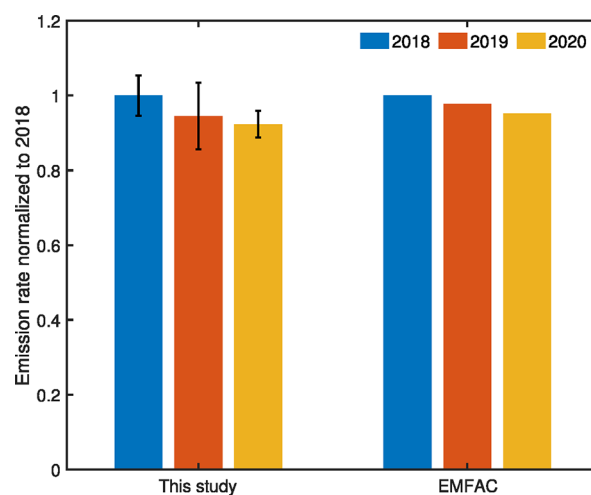


Figure 6. Emission rate per vehicle derived in this study and estimated from the CARB EMFAC 2017 model. Each year is normalized to 2018. The whiskers represent the 1σ uncertainty.

model. From the observations, we infer a $7.6 \pm 3.5\%$ reduction in the CO₂ emission rate per vehicle from 2018 to 2020 (two-sample *t*-test, *p*-value < 0.001). Uncertainties in the 2019 year are large because the data available for the analysis was small that year (see Table 1). Despite the larger noise, the

Table 1. Derived q ,^a 1 σ Uncertainty, and Data Reliability Statistics for Each Year

		2018	2019	2020
before removing biogenic CO ₂	emission rate (10 ⁻⁶ kg CO ₂ m ⁻¹ per veh.)	283	360	264
	1 σ uncertainty (%)	6.7	7.1	8.1
after removing biogenic CO ₂	emission rate (10 ⁻⁶ kg CO ₂ m ⁻¹ per veh.)	298	281	275
	1 σ uncertainty (%)	5.4	9.4	3.9
data reliability statistics	number of sites	15	14	17
	average days of data availability	168	100	278

^a q is calculated from q/α assuming 0.15 for α .

normalized value for 2019 is intermediate between 2018 and 2020 and consistent with the overall trend. The trend is also consistent, within the uncertainty bounds, of the slightly smaller 4.7% reduction for 2018 through 2020 estimated from the CARB EMFAC 2017 model. Considering the fact that vehicle miles traveled (VMT) increased by 1% between 2018 and 2019,²² this observational estimate of fuel efficiency suggests the State of California's goal of 3%/year decrease in mobile emissions is being achieved on-road. In 2020, VMT decreased by 14.5% due to the shelter-in-place order in California. Combining this reduction with the improved fuel efficiency that we infer from the observations indicates that an 18% decrease in annual mobile emissions compared to the previous year occurred in 2020.

In this analysis, we demonstrate an approach to combining a large number of densely spaced observations with a Gaussian plume model for quantifying annual trends in vehicular CO₂ emission rates. The approach is not computationally demanding and could easily be adapted to other gases (e.g., CO, NO_x, and primary aerosol). Elements needed for the success of this approach include a dense network with near highway observations, measurements or models of meteorological parameters, and measurements of traffic flow. Not surprisingly, the high uptime of the observations, including a larger number of locations sites and increased data availability at each site, improves the precision of the analysis. The higher signal-to-noise ratio of 2020 compared to 2019 reinforces that point. A concerted effort during the 2020 year led to a substantial increase in data, despite the challenges of instrument maintenance during the pandemic. The results are also more precise when we separate distinct meteorological periods. Here, we use the PBLH as a surrogate for that variation. In addition, because of covariance between traffic flow and biogenic emissions and uptake, estimating the signal from biogenic emissions and removing them prior to the attribution of a traffic signal improves the signal-to-noise ratio.

The analysis here provides guidance for understanding the changing landscape of vehicle CO₂ emissions. Additional analyses will be needed to establish whether it is because of increased purchases of electric vehicles or increases in the use

of more fuel-efficient gasoline vehicles. The analysis of vehicle CO₂ efficiency trends in multiple cities will also help to understand whether improvements are uniform or accelerated by local policies. The BEACO₂Ns with 12–25 nodes have recently been installed in Los Angeles, CA and Glasgow, Scotland, offering the opportunity to compare with the changes we infer from the San Francisco Bay Area network. We look forward to comparable analyses for other gases and aerosols emitted by traffic and to other new approaches to interpreting observations from dense networks such as the BEACO₂N or the much denser Purple Air.

■ ASSOCIATED CONTENT

Supporting Information

The Supporting Information is available free of charge at <https://pubs.acs.org/doi/10.1021/acs.est.1c06828>.

Detailed description of the design and deployment of the BEACO₂N, estimation of the biogenic CO₂ signal, and additional discussion of the effect of the PBLH variation on the analysis (PDF)

■ AUTHOR INFORMATION

Corresponding Author

Ronald C. Cohen – Department of Earth and Planetary Science and Department of Chemistry, University of California, Berkeley, Berkeley, California 94720, USA; orcid.org/0000-0001-6617-7691; Email: rccohen@berkeley.edu

Authors

Jinsol Kim – Department of Earth and Planetary Science, University of California, Berkeley, Berkeley, California 94720, USA; Present Address: Department of Earth Science, University of Southern California, Los Angeles, CA 90007, United States; orcid.org/0000-0002-7780-0685

Alexander J. Turner – Department of Earth and Planetary Science, University of California, Berkeley, Berkeley, California 94720, USA; Present Address: Department of Atmospheric Sciences, University of Washington, Seattle, WA 98195, United States.

Helen L. Fitzmaurice – Department of Earth and Planetary Science, University of California, Berkeley, Berkeley, California 94720, USA; orcid.org/0000-0002-1631-5491

Erin R. Delaria – Department of Chemistry, University of California, Berkeley, Berkeley, California 94720, USA; Present Address: NASA Goddard Space Flight Center, Greenbelt, MD 20771, United States.; orcid.org/0000-0002-6033-848X

Catherine Newman – Department of Chemistry, University of California, Berkeley, Berkeley, California 94720, USA

Paul J. Wooldridge – Department of Chemistry, University of California, Berkeley, Berkeley, California 94720, USA

Complete contact information is available at: <https://pubs.acs.org/doi/10.1021/acs.est.1c06828>

Notes

The authors declare no competing financial interest.

■ ACKNOWLEDGMENTS

This research was funded by a grant from the Koret Foundation. This research used the Savio computational

cluster resource provided by the Berkeley Research Computing program at the University of California, Berkeley (supported by the UC Berkeley Chancellor, Vice Chancellor for Research, and Chief Information Officer). Additional support was provided by the Kwanjeong Educational Fellowship to Jinsol Kim, the UC Berkeley Miller Postdoctoral Fellowship to A.J.T., and both the NSF GRFP fellowship and the Microsoft Research Internship to Helen Fitzmaurice.

REFERENCES

- (1) *California's 2017 Climate Change Scoping Plan*; California Air Resources Board, 2017.
- (2) *California Greenhouse Gas Emissions for 2000 to 2017: Trends of Emissions and Other Indicators*; California Air Resources Board, 2017.
- (3) *2017 Clean Air Plan: Spare the Air, Cool the Climate*; Bay Area Air Quality Management District, 2017.
- (4) Gately, C. K.; Hutyra, L. R. Large Uncertainties in Urban-Scale Carbon Emissions. *J. Geophys. Res.: Atmos.* **2017**, *122*, 11,242–11,260.
- (5) Heimbürger, A. M. F.; Harvey, R. M.; Shepson, P. B.; Stirn, B. H.; Gore, C.; Turnbull, J.; Cambaliza, M. O. L.; Salmon, O. E.; Kerlo, A.-E. M.; Lavoie, T. N.; Davis, K. J.; Lauvaux, T.; Karion, A.; Sweeney, C.; Brewer, W. A.; Hardesty, R. M.; Gurney, K. R. Assessing the Optimized Precision of the Aircraft Mass Balance Method for Measurement of Urban Greenhouse Gas Emission Rates through Averaging. *Elementa* **2017**, *5*, 26.
- (6) Turnbull, J. C.; Karion, A.; Davis, K. J.; Lauvaux, T.; Miles, N. L.; Richardson, S. J.; Sweeney, C.; McKain, K.; Lehman, S. J.; Gurney, K. R.; Patarasuk, R.; Liang, J.; Shepson, P. B.; Heimbürger, A.; Harvey, R.; Whetstone, J. Synthesis of Urban CO₂ Emission Estimates from Multiple Methods from the Indianapolis Flux Project (INFLUX). *Environ. Sci. Technol.* **2019**, *53*, 287–295.
- (7) Newman, S.; Xu, X.; Gurney, K. R.; Hsu, Y. K.; Li, K. F.; Jiang, X.; Keeling, R.; Feng, S.; O'Keefe, D.; Patarasuk, R.; Wong, K. W.; Rao, P.; Fischer, M. L.; Yung, Y. L. Toward consistency between trends in bottom-up CO₂ emissions and top-down atmospheric measurements in the Los Angeles megacity. *Atmos. Chem. Phys.* **2016**, *16*, 3843–3863.
- (8) Lauvaux, T.; Gurney, K. R.; Miles, N. L.; Davis, K. J.; Richardson, S. J.; Deng, A.; Nathan, B. J.; Oda, T.; Wang, J. A.; Hutyra, L.; Turnbull, J. Policy-Relevant Assessment of Urban CO₂ Emissions. *Environ. Sci. Technol.* **2020**, *54*, 10237–10245.
- (9) Sargent, M.; Barrera, Y.; Nehrkorn, T.; Hutyra, L. R.; Gately, C. K.; Jones, T.; McKain, K.; Sweeney, C.; Hegarty, J.; Hardiman, B.; Wang, J. A.; Wofsy, S. C. Anthropogenic and biogenic CO₂ fluxes in the Boston urban region. *Proc. Natl. Acad. Sci. U.S.A.* **2018**, *115*, 7491–7496.
- (10) Yadav, V.; Ghosh, S.; Mueller, K.; Karion, A.; Roest, G.; Gourdj, S. M.; Lopez-Coto, I.; Gurney, K. R.; Parazoo, N.; Verhulst, K. R.; Kim, J.; Prinzivalli, S.; Fain, C.; Nehrkorn, T.; Mountain, M.; Keeling, R. F.; Weiss, R. F.; Duren, R.; Miller, C. E.; Whetstone, J. The Impact of COVID-19 on CO₂ Emissions in the Los Angeles and Washington DC/Baltimore Metropolitan Areas. *Geophys. Res. Lett.* **2021**, *48*, 1–10.
- (11) Staufer, J.; Broquet, G.; Bréon, F.-M.; Puygrenier, V.; Chevallier, F.; Xueref-Rémy, I.; Dieudonné, E.; Lopez, M.; Schmidt, M.; Ramonet, M.; Perrussel, O.; Lac, C.; Wu, L.; Ciais, P. The first 1-year-long estimate of the Paris region fossil fuel CO₂ emissions based on atmospheric inversion. *Atmos. Chem. Phys.* **2016**, *16*, 14703–14726.
- (12) Delaria, E. R.; Kim, J.; Fitzmaurice, H. L.; Newman, C.; Wooldridge, P. J.; Worthington, K.; Cohen, R. C. The Berkeley Environmental Air-quality and CO₂ Network: field calibrations of sensor temperature dependence and assessment of network scale CO₂ accuracy. *Atmos. Meas. Tech.* **2021**, *14*, 5487–5500.
- (13) Kim, J.; Shusterman, A. A.; Lieschke, K. J.; Newman, C.; Cohen, R. C. The BERkeley Atmospheric CO₂ Observation Network: field calibration and evaluation of low-cost air quality sensors. *Atmos. Meas. Tech.* **2018**, *11*, 1937–1946.
- (14) Shusterman, A. A.; Teige, V. E.; Turner, A. J.; Newman, C.; Kim, J.; Cohen, R. C. The BERkeley Atmospheric CO₂ Observation Network: initial evaluation. *Atmos. Chem. Phys.* **2016**, *16*, 13449–13463.
- (15) Shusterman, A. A.; Kim, J.; Lieschke, K. J.; Newman, C.; Wooldridge, P. J.; Cohen, R. C. Observing local CO₂ sources using low-cost, near-surface urban monitors. *Atmos. Chem. Phys.* **2018**, *18*, 13773–13785.
- (16) Turner, A. J.; Shusterman, A. A.; McDonald, B. C.; Teige, V.; Harley, R. A.; Cohen, R. C. Network design for quantifying urban CO₂ emissions: assessing trade-offs between precision and network density. *Atmos. Chem. Phys.* **2016**, *16*, 13465–13475.
- (17) Turner, A. J.; Kim, J.; Fitzmaurice, H.; Newman, C.; Worthington, K.; Chan, K.; Wooldridge, P.; Köhler, P.; Frankenberg, C.; Cohen, R. C. Observed Impacts of COVID-19 on Urban CO₂ Emissions. *Geophys. Res. Lett.* **2020**, *47*, No. e2020GL090037.
- (18) Choi, W.; Winer, A. M.; Paulson, S. E. Factors Controlling Pollutant Plume Length Downwind of Major Roadways in Nocturnal Surface Inversions. *Atmos. Chem. Phys.* **2014**, *14*, 6925–6940.
- (19) Briggs, G. A. *Diffusion Estimation for Small Emissions*; U.S. Department of Energy, 1973.
- (20) Dee, D. P.; Uppala, S. M.; Simmons, A. J.; Berrisford, P.; Poli, P.; Kobayashi, S.; Andrae, U.; Balmaseda, M. A.; Balsamo, G.; Bauer, P.; Bechtold, P.; Beljaars, A. C. M.; van de Berg, L.; Bidlot, J.; Bormann, N.; Delsol, C.; Dragani, R.; Fuentes, M.; Geer, A. J.; Haimberger, L.; Healy, S. B.; Hersbach, H.; Hólm, E. V.; Isaksen, I.; Kållberg, P.; Köhler, M.; Matricardi, M.; McNally, A. P.; Monge-Sanz, B. M.; Morcrette, J.-J.; Park, B.-K.; Peubey, C.; de Rosnay, P.; Tavolato, C.; Thépaut, J.-N.; Vitart, F. The ERA-Interim Reanalysis: Configuration and Performance of the Data Assimilation System. *Q. J. R. Meteorol. Soc.* **2011**, *137*, 553–597.
- (21) CARB EMFAC. <https://arb.ca.gov/emfac/emissions-inventory> (accessed Jan 04, 2021).
- (22) Caltrans Pems. <https://pems.dot.ca.gov/> (accessed Aug 17, 2021).